J|A|C|S
ARTICLES
Published on Web 11/19/2003

Propagation of Melting Cooperativity along the Phosphodiester Backbone of DNA

Jessica Becaud, Isabelle Pompizi, and Christian J. Leumann*

Contribution from the Department of Chemistry and Biochemistry, University of Bern, Freiestrasse 3, CH-3012 Bern, Switzerland

Received March 25, 2003; E-mail: leumann@ioc.unibe.ch

Abstract: The role of the DNA phosphodiester backbone in the transfer of melting cooperativity between two helical domains was experimentally addressed with a helix−bulge−helix DNA model, in which the bulge consisted of a varying number of either conformationally flexible propanediol or conformationally constrained bicyclic anucleosidic phosphodiester backbone units. We found that structural communication between two double helical domains is transferred along the DNA backbone over the equivalent of ca. 12−20 backbone units, depending on whether there is a symmetric or asymmetric distribution of the anucleosidic units on both strands. We observed that extension of anucleosidic units on one strand only suffices to disrupt cooperativity transfer in a similar way as if extension occurs on both strands, indicating that the length of the longest anucleosidic inset determines cooperativity transfer. Furthermore, conformational rigidity of the sugar unit increases the distance of coopertivity transfer along the phosphodiester backbone. This is especially the case when the units are asymmetrically distributed in both strands.

Introduction

The assembly of two nucleic acid single strands into a double helix via Watson−Crick base-pair formation is a highly cooperative process. The generally accepted mechanistic model for DNA duplex formation from two single strands consists of an endothermal helix nucleation step followed by exothermal helix propagation steps.[1] On the molecular level, the cooperativity of this process is determined by the stacking interactions of consecutively formed base pairs and by the nature and conformational properties of the sugar−phosphate backbone.

The effect of base stacking on the cooperativity of DNA duplex formation was investigated before via chemical ligation of a reporter oligonucleotide to its template in the presence and absence of a third oligonucleotide bound adjacently to the template.[2−4] It was shown that two pyrimidine bases at the junction site lead to no increase in the binding constant of the reporter oligonucleotide, while a 28-fold enhancement was observed when two guanines are next to each other, indicating a considerable positive cooperative effect for strand association mediated by purine stacking.[4] A similar situation is encountered in DNA triplex formation of two adjacent pyrimidine strands on a DNA duplex template. Here, binding enhancements of 12−127-fold were observed depending on the nature of the (pyrimidine) bases at the junction site.[5]

The contribution of the backbone structure on cooperativity of duplex formation, however, is largely unknown, and experimental investigations specifically addressing this question are rare. A thermochemical analysis of an abasic and anucleosidic DNA duplex revealed that the stability loss of such a DNA lesion primarily results from removal of the base. However, the cooperativity of the melting process remained largely unaffected by such a lesion, implying that the phosphodiester backbone, rather than the base−sugar network, serves as the primary propagation path for the communication of cooperative melting effects.[6] A similar investigation on a duplex containing a bistrand lesion (two abasic sites in the duplex opposing each other) revealed again no alteration in duplex melting cooperativity, thus supporting this notion.[7]

Single-stranded, functional RNA (and DNA) as occurring after DNA transcription or in (deoxy)ribozymes and aptamers form highly folded structures with double helical stretches that are connected via bulges or loops as the most common secondary structural motifs.[8,9] Especially for aptamers, it is known that the ligand-binding event is often associated with an adaptive binding mechanism, in which substantial structural reorganization of the RNA occurs in a highly cooperative way.[10] To correlate structure with function it is therefore important to understand how double helical regions that are interrupted by

(1) Cantor, C. R.; Schimmel, P. R. Nucleic Acid Structural Transitions; In *Biophysical Chemistry Part III: The Behavior of Biological Macromolecules*; Vapnek, P. C., Ed.; W. H. Freeman: New York, 1980; Chapter 23.
(2) Adeenah-Zadah, A.; Knorre, D. G.; Fedorova, O. S. *J. Biomol. Struct. Dyn.* **1997**, *15*, 369−380.
(3) Fedorova, O. S.; Adeenah-Zadah, A.; Bichenkova, E. V.; Knorre, D. G. *J. Biomol. Struct. Dyn.* **1995**, *13*, 145−166.
(4) Koval, V. V.; Lokteva, N. A.; Karnaukhova, S. L.; Fedorova, O. S. *J. Biomol. Struct. Dyn.* **1999**, *17*, 259−265.
(5) Colocci, N.; Dervan, P. B. *J. Am. Chem. Soc.* **1995**, *117*, 4781−4787.
(6) Vesnaver, G.; Chang, C.-N.; Eisenberg, M.; Grollman, A. P.; Breslauer, K. J. *Proc. Natl. Acad. Sci. U.S.A.* **1989**, *86*, 3614−3618.
(7) Gelfand, C. A.; Plum, G. E.; Grollman, A. P.; Johnson, F.; Breslauer, K. J. *Biopolymers* **1996**, *38*, 439−445.
(8) Pace, N. R.; Thomas, B. C.; Woese, C. R. In *The RNA World*; Gesteland, R. F.,
(8) Cech, T. R., Atkins, J. F., Eds.; Cold Spring Harbor Laboratory Press: Plainview, NY, 1999; pp 113−141.
(9) Batey, R. T.; Rambo, R. P.; Doudna, J. A. *Angew. Chem., Int. Ed.* **1999**, *38*, 2326−2343.
(10) Hermann, T.; Patel, D. J. *Science* **2000**, *287*, 820−825.

10.1021/ja035313j CCC: $25.00 **© 2003 American Chemical Society**

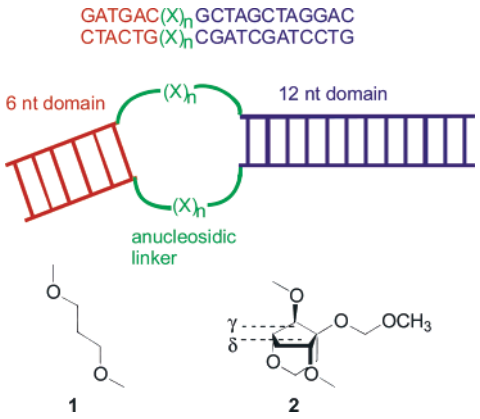

Figure 1. Sequence information and design of the helix−bulge−helix system consisting of a 6-nt and a 12-nt duplex domain, interrupted by conformationally unconstrained (**1**) or constrained (**2**) anucleosidic units (n = 1, 2, 3, 6, 9, 12, 16, 20).

loops or bulges communicate with each other and influence each other's properties.

In this context, we set out to investigate the dependence of duplex melting cooperativity between two double helical domains on the length and the conformational properties of the intervening sugar−phosphate backbone in a model system. To this end, we designed an oligodeoxynucleotide duplex containing a 6-nucleotide (nt) and a 12-nt base-paired domain that is interrupted via 1−20 anucleosidic backbone units **1** or **2** (Figure 1). Both anucleosidic units contain the same number of backbone bonds as a regular deoxynucleoside unit. They differ, however, in their conformational flexibility. While the propanediol linker **1** is conformationally unconstrained, the bicyclic unit **2** shows locked geometry for the two C−C bonds representing the C(5′)−C(4′) and C(4′)−C(3′) bond of a deoxynucleoside (torsion angles γ and δ). We have used this basic scaffold previously in the context of the DNA analogue bicyclo[3.2.1]-DNA.[11,12] Its geometry matches that of a nucleoside unit in a B-DNA duplex.[13] UV melting curve analysis was used for monitoring melting cooperativity. The two helical domains are different in size and thermal stability and designed to show two independent melting transitions in the absence of cooperativity transfer from one unit to the other.

Results and Discussion

Although the building block for incorporation of **1** is known,[6,14] that for the bicyclic unit **2** (**7**) was synthesized in four steps (Scheme 1), starting from precursor **3** for which we already developed a synthetic access.[11] Oligonucleotides were prepared and analyzed by established methodology (see Experimental Section).

Symmetric Duplexes. First, we investigated the melting behavior of oligonucleotides containing one or two units of **1** and **2** at opposite positions by means of UV melting curve analysis and determined the thermodynamic data (Table 1) for n = 0−2, via a standard curve-fitting procedure to the experimental melting curve. Extraction of relevant thermodynamic data for n > 2 in this way seems unreasonable due to the expected breakdown of the two-state melting model.

Scheme 1 [a]

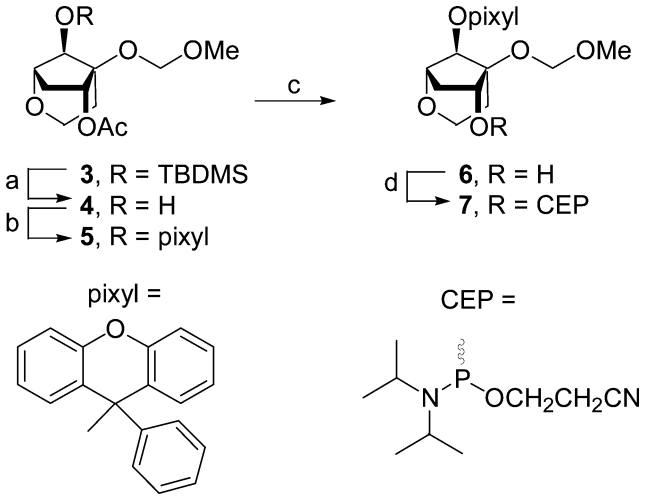

[a] Reagents and yields: (a) Bu_4NF, THF, rt, 4h, 93%. (b) 9-Chloro-9-phenylxanthene, pyridine, rt, 16h, 95%. (c) NaOH (0.2 M) in THF/MeOH/H_2O, 5:4:1, rt, 45 min, quant. (d) ClP[(OCH2CH2CN)($NiPr_2$)], $^iPr_2NEt$, THF, rt, 6h, 91%.

Table 1. T_m and Thermodynamic Data from UV Melting Curves (260 nm) of Duplexes as Depicted in Figure 1[a]

n	X	T_m [°C]	ΔH^{fit} [kcal·mol^{-1}]	ΔS^{fit} [cal·mol^{-1}·K^{-1}]	$\Delta G^{fit(25\ °C)}$ [kcal·mol^{-1}]
0		64.0	−111.3	−303.6	−20.8
1	**1**	53.6	−111.5	−312.5	−18.1
2	**1**	48.7	−81.9	−227.0	−14.3
1	**2**	52.0	−116.3	−330.5	−17.8
2	**2**	48.2	−96.9	−274.8	−15.0

[a] Duplex concentration: 1.8−2.0 μM, in 0.15 mM NaH_2PO_4, 150 mM NaCl, pH 7.0.

As can be seen from Table 1, the introduction of one pair of anucleosidic units **1** or **2** leads to a considerable thermal and thermodynamic destabilization of the duplex. The destabilization is not reflected in the enthalpy term (cf. duplex with n = 0) and is therefore entirely entropic in nature. This is in full agreement with earlier observations[7] and is a strong indication of an intact base stack, bypassing the anucleosidic sites (anucleosidic residues looped out). Introduction of a second pair of anucleosidic units (n = 2) leads to a further, though less pronounced, reduction in T_m. Here, the additional destabilization is accompanied by a reduction of the enthalpy term and is thus an indication for the rupture of the base stack at the anucleosidic site. Reduced stacking efficiency is corroborated by the sharp reduction in hypochromicity of the melting process for n = 2 compared to n = 1 (Figure 2). There are no significant differences in thermal duplex destabilization between anucleosidic units **1** and **2**. The enthalpy data show consistently more negative values in the case of the conformationally constrained **2** which, however, does not significantly affect ΔG. Thus, the loss of thermodynamic stability is largely independent of the conformational rigidity of the backbone at the anucleosidic sites. Extension of the anucleosidic loop from n = 3 to up to n = 20 does not further influence the T_m, in the case of neither **1** nor **2** as the anucleosidic sites.

The first derivatives of the melting curves (Figure 2) clearly show two separate maxima for n > 16, corresponding to two independent transitions with T_m1 = 26 ± 1 °C in the case of

(11) Epple, C.; Leumann, C. *Chem. Biol.* **1998**, *5*, 209−216.
(12) Keller, B. M.; Leumann, C. J. *Angew. Chem., Int. Ed.* **2000**, *39*, 2278−2281.
(13) Epple, C.; Leumann, C.; Stoeckli-Evans, H. *Acta Crystallogr., Sect. C* **1998**, *54*, 1141−1143.
(14) Seela, F.; Kaiser, K. *Nucleic Acids Res.* **1987**, *15*, 3113−3129.

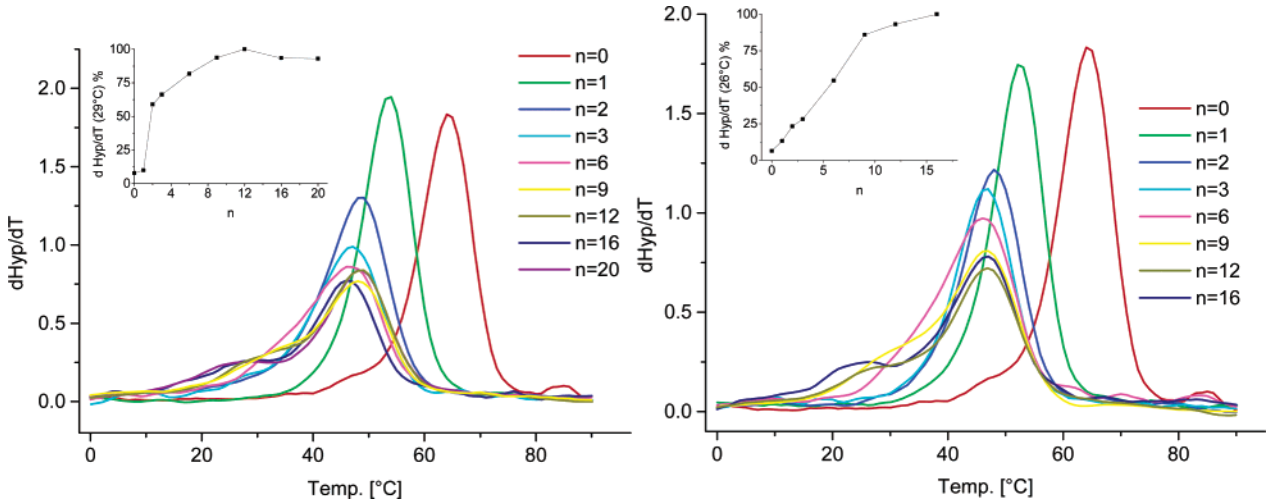

Figure 2. First derivatives of the melting curves (260 nm) for the duplexes given in Figure 1, containing varying (*n*) consecutive anucleosidic units X = **1** (left) and X = **2** (right). The insets represent a plot of dHyp/dT vs *n* at the T_m of the transition of the hexamer domain (26 °C for **2** and 29 °C for **1**) as a function of the number of anucleosidic units *n*. Experimental conditions as described in Table 1.

anucleosidic unit **2** or 29 ± 1 °C for unit **1** and T_m2 = 47 ± 1 °C for both cases. T_m1 corresponds to the melting of the hexamer domain while T_m2 represents the melting of the dodecamer domain. This clearly demonstrates that the melting of the hexamer domain is completely decoupled from the melting of the dodecamer domain in these cases.

As a control, we prepared the duplexes corresponding to the isolated hexamer and dodecamer domains. The corresponding T_m's are 8.9 and 49.0 °C, respectively. The difference in the T_m's of the hexamer domain and the isolated hexamer duplex can be explained by the fact that the melting process of the former is monomolecular. To prove that the hexamer domains are involved in complementary base pairing in the duplexes with *n* = 2, 3, and 6, a hexanucleotide that is complementary to either the first or the second strand of the hexamer domain was added. The absence of an additional transition clearly ruled out the possibility of the hexamer domains to be unpaired in these cases (data not shown).

To analyze the extent of the backbone transmitted cooperativity in the melting of the hexamer domain as a function of the number of intervening anucleosidic units *n* in more detail, we plotted a cross section of the normalized dHyp/dT data at the T_m2 of the hexamer domain (26 °C for X = **2**, 29 °C for X = **1**) as a function of *n* (insets in Figure 2), reasoning that the rise in hyperchromicity at T_m1 is proportional to the fraction of the hexamer domain, melting as a separate, isolated cooperative unit. In this approximation, 100% indicates complete decoupling (two independent transitions for each domain observable) and 0% melting as a single fully cooperative unit (no hyperchromicity at the temperature of T_m1 detectable). According to this analysis, cooperativity in the melting process of the two domains ends at *n* between 12 and 16, independent of the nature of the anucleosidic unit. The values for duplexes with *n* = 1 are similar for both anuceosidic units **1** and **2** and near to 0. This is indicative for a melting process as one cooperative unit in both cases. Differences in the two systems arise, however, for $n \geq 2$, where the normalized dHyp/dT data for unit **1** indicate already partial decoupling of the two base-pairing domains, while this is not the case for unit **2**. The 50% level of decoupling is reached at *n* = 2−3 for X = **1** and *n* = 6 for X = **2**. Thus, it emerges that there is no difference in the overall distance of cooperativity transmission as a function of the conformational flexibility of the phosphodiester backbone. However, decoupling rises less steeply in the case of the conformationally constrained backbone unit **2** as compared to the conformationally flexible backbone unit **1**.

Asymmetric Duplexes. Given the fact that internal bulges in nucleic acid structures in most cases contain an asymmetric distribution of nucleotide residues on either strand, we became interested in the question how an asymmetric distribution of unit X in both strands would influence the cooperativity transfer. To this end, we investigated duplexes in which the number of X in one strand was kept fixed at *n* = 2, while *n* was varied for the other strand and vice versa. This analysis was again performed for both the propanediol (X = **1**) and the bicyclic (X = **2**) anucleosidic units, giving a total of four datatsets. The first derivatives of the corresponding melting curves with the normalized dHyp/dT insets, as described before, are reproduced in Figure 3.

We chose *n* = 2 for the nonvaried strands to exclude intrastrand stacking contributions to cooperativity propagation. Again we measured the rise of hyperchromicity at the T_m1 (30 °C). For the case of the flexible unit X = **1**, the arrangement of *n* = 2, 3 indicated more than 50% loss of cooperativity transfer, which was expected on the basis of the symmetric system, where *n* = 2 showed already a similar behavior (Figure 3, left). Complete decoupling of the two melting domains was observed for the systems *n* = 2, >12. As expected, we observed no significant differences as to in which of the two strands *n* was kept constant.

The picture is different for the case of the conformationally restricted anucleosidic unit X = **2** (Figure 3, right). In these cases, the shortest intervening stretches (*n* = 2, 3) of anucleosidic units lead only to a decrease in cooperativity transfer of 25% or less. After extending one chain to 16 units of **2**, cooperativity transfer is mostly but not completely interrupted. Also in this case there was no difference as to whether *n* was kept fixed at strand 1 or 2.

The two most relevant observations from these experiments are: (i) extending anucleosidic units on one chain only suffices to disrupt cooperativity transfer approximately to the same extent as if the extension occurs on both strands in the case of the

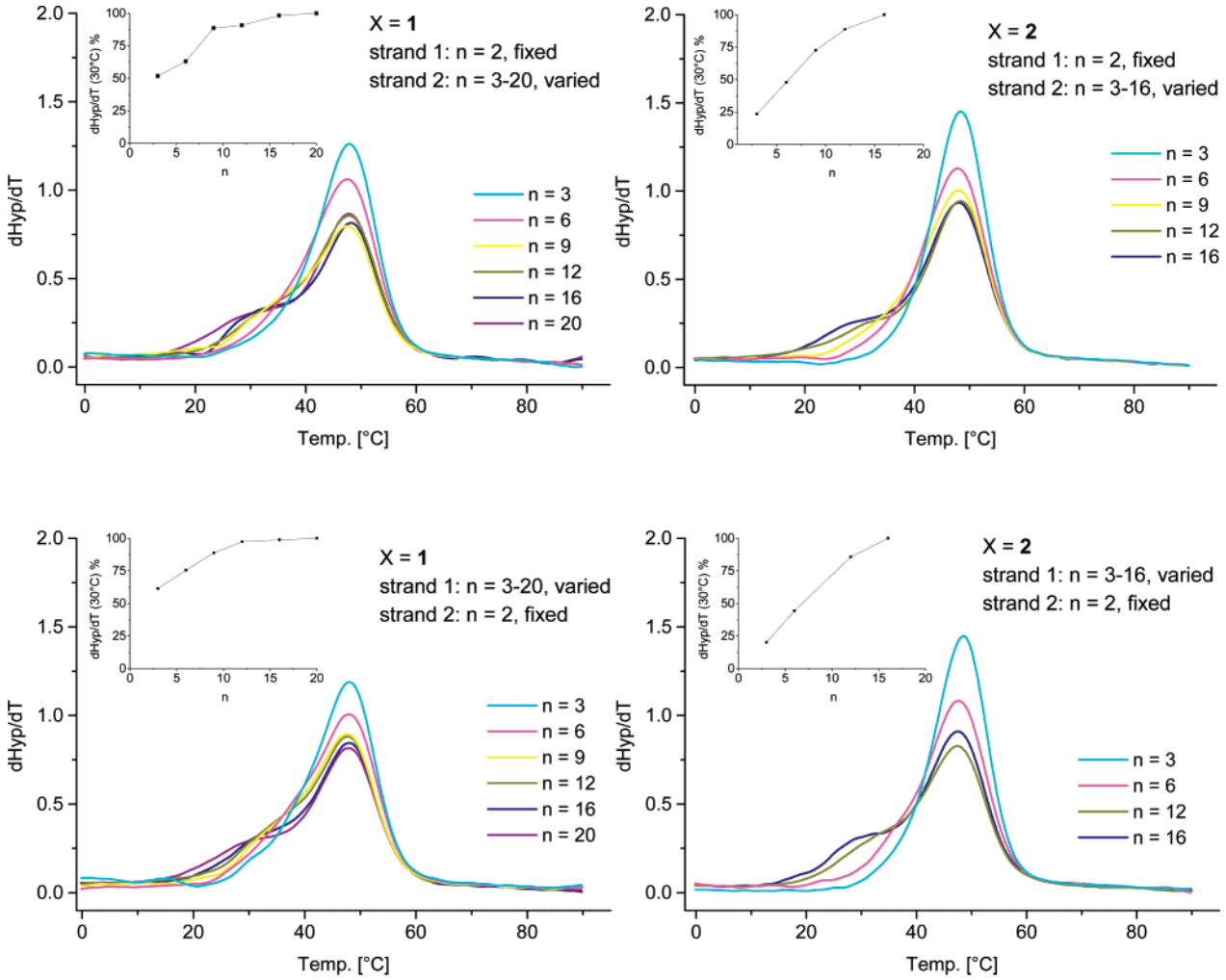

Figure 3. First derivatives of the melting curves (260 nm) for the duplexes given in Figure 1, containing an asymmetric distribution of consecutive anucleosidic units *n*. The insets represent a plot of dHyp/dT vs *n* at the T_m of the transition of the hexamer domain (30 °C) as a function of the number of anucleosidic units *n*. Experimental conditions as described in Table 1.

flexible unit **1** and (ii) conformational rigidity leads to transfer of cooperativity over longer distances ($n > 16$), as observed for the asymmetric duplexes containing **2**.

Conclusions

On the example of duplex melting, we demonstrated here for the first time that structural communication between two double helical domains is transferred along the DNA backbone over the equivalent of ca. 12−20 backbone units, depending on whether there is a symmetric or asymmetric distribution of the anucleosidic units on both strands. We observed that extension of anucleosidic units on one strand solely suffices to disrupt cooperativity transfer in a similar way as if extension occurs on both strands, indicating that the length of the longest anucleosidic inset determines cooperativity transfer. Furthermore, conformational rigidity of the sugar unit increases the distance of cooperativity transfer along the phosphodiester backbone. This is especially the case when the units are asymmetrically distributed in both strands. This information is useful in understanding remote structural and functional correlation in ribosomal or mRNA or in RNA and DNA enzymes and aptamers. It will also be of interest in the design of functional ribozymes or aptamers consisting of mixed backbone structures.[15]

This study was aimed at investigating the role of the phosphodiester backbone in cooperativity transfer exclusively. The real situation in nucleic acid secondary structures is certainly more complicated, as the presence of bases in bulges will contribute to the cooperativity transfer, for example, via intrastrand stacking effects. Such effects can be addressed in the same way as described here, by replacing the anucleosidic units by nonpairing nucleotide units and by refining the analysis of cooperativity transfer by utilizing, for example, fluorescence techniques with adequately positioned fluorophores and quenchers.

Experimental Section

General. ^{1}H NMR (300 MHz), ^{13}C NMR (75 MHz): Bruker AC-300; δ = ppm relative to residual undeuterated solvent; J = Hz. Carbon multiplicity (s, d, t, q) from DEPT. LSIMS and EI mass spectra: AutoSpeq Q VG at 70 eV. ESI-MS mass spectra: Fisons Instrument VG Platform. IR spectroscopy: Perkin-Elmer FTIR 1600, ν = cm^{-1}. Flash chromatography (FC) was performed with Silica Gel 60 (particles size 40−63 μm) from Fluka. All chemicals were reagent grade from Acros, Fluka, and Aldrich. Solvents were of technical quality and distilled prior to use.

(15) Ackermann, D.; Wu, X.; Pitsch, S. *Helv. Chim. Acta* **2002**, *85*, 1463−1478.

(1*S*,5*S*,6*R*,8*S*)-6-Acetoxy-5-[(methoxymethyl)oxy]-2-oxabicyclo-[3.2.1]octan-8-ol (4). To a solution of **3** (745 mg, 2.07 mmol) in THF (10 mL) was added $Bu_4NF{\cdot}3H_2O$ (782 mg, 2.48 mmol), and the resulting mixture was stirred for 4 h at rt. Then the mixture was diluted with EtOAc (10 mL) and extracted with saturated $NaHCO_3$ (10 mL). The aqueous phase was washed twice with EtOAc (10 mL), and the combined organic phases were dried ($MgSO_4$) and evaporated. FC (hexane/EtOAc, 2:3) gave **4** (472 mg, 93%) as a colorless oil.

TLC (hexane/EtOAc, 1:2): Rf = 0.39. ^{1}H NMR (300 MHz, $CDCl_3$): δ 1.64 (*ddd*, *J* = 15.8, *J* = 3.7, *J* = 1.5, 1H); 1.82−1.93 (*m*, 1H); 1.94−2.03 (*m*, 1H); 2.08 (*s*, 3H); 2.77 (*ddd*, *J* = 16.2, *J* = 10.7, *J* = 5.9, 1H); 3.42 (*s*, 3H); 3.69−3.94 (*m*, 3H); 4.17 (*dd*, *J* = 5.5, *J* = 1.1, 1H); 4.73, 4.78 (2*d*, *J* = 7.3, 2H); 5.38 (*dd*, *J* = 10.6, *J* = 3.7, 1H). ^{13}C NMR (75 MHz, $CDCl_3$): δ 20.97 (*q*); 31.50 (*t*); 32.82 (*t*); 55.66 (*q*); 59.56 (*t*); 74.60 (*d*); 76.76 (*d*); 78.50 (*d*); 85.47 (*s*); 91.55 (*t*); 170.50 (*s*). IR ($CHCl_3$): 3453 *m*, 3048 *w*, 2959 *s*, 2828 *m*, 1732 *s*, 1482 *m*, 1433 *m*, 1376 *m*, 1303 *w*, 1266 *s*, 1190 *m*, 1094 *s*, 902 *m*, 858 *m*, 824 *m*. MS (LSIMS): 247 (14, $M^+ + 1$), 215 (43), 185 (8), 167 (7), 155 (23), 149 (10), 138 (32), 137 (67), 125 (100), 120 (15), 109 (18), 107 (37), 105 (15).

(1*S*,5*S*,6*R*,8*S*)-6-Acetoxy-5-[(methoxymethyl)oxy]-8-[9′-(9′-phenylxanthenyl)oxy]-2-oxabicyclo[3.2.1]octan (5). To a solution of **4** (100 mg, 0.41 mmol) in dry pyridine (1 mL) was added 9-chloro-9-phenylxanthene (240 mg, 0.82 mmol), and the mixture was stirred for 16h at rt. After being diluted with CH_2Cl_2 (5 mL), extracted with saturated $NaHCO_3$ (5 mL), and washed of the aqueous phase twice with CH_2Cl_2 (5 mL), the combined organic phases were dried (Na_2SO_4) and evaporated, and the crude product was adsorbed on silicagel (1 g) and purified by FC (hexane/EtOAc, 4:1, 1% Et_3N) to give **5** (197 mg, 95%) as a white foam.

TLC (hexane/EtOAc, 7:3): Rf = 0.45. ^{1}H NMR (300 MHz, $CDCl_3$): δ 1.44 (*ddd*, *J* = 15.8, *J* = 3.7, *J* = 1.8, 1H); 1.59−1.70 (*m*, 1H); 2.00−2.07 (*m*, 4H); 2.67 (*ddd*, *J* = 16.2, *J* = 10.7, *J* = 5.9, 1H); 3.00 (*d*, *J* = 4.8. 1H); 3.26 (*s*, 3H); 3.31−3.33 (*m*, 1H); 3.49−3.68 (*m*, 2H); 4.26, 4.47 (2*d*, *J* = 7.3, 2H); 5.45 (*dd*, *J* = 10.3, *J* = 3.3, 1H); 6.93−7.43 (*m*, 13H). ^{13}C NMR (75 MHz, $CDCl_3$): δ 21.03 (*q*); 32.79 (*t*); 33.21 (*t*); 55.04 (*q*); 59.38 (*t*); 76.04 (*d*); 76.20 (*s*); 77.02 (*d*); 79.69 (*d*); 83.61 (*s*); 92.22 (*t*); 116.19, 116.55 (2*d*); 123.16, 123.32 (2*d*); 124.02 (*s*); 127.21, 127.70, 129.53, 129.71, 130.71, 131.52 (6*d*); 148.33, 151.02, 151.61 (3*d*); 170.65 (*s*). IR ($CHCl_3$): 3038 *w*, 2956 *m*, 2893 *m*, 2824 w, 1732 *s*, 1603 *m*, 1574 *m*, 1479 *s*, 1448 *s*, 1377 *m*, 1319 *s*, 1297 *s*, 1244 *s*, 1148 *m*, 1120 *m*, 1101 *s*, 979 *m*, 939 *m*, 910 *m*, 874 *m*, 832 *w*. MS (LSIMS): 503 (<1, $M^+ + 1$), 460 (<1), 257 (100), 107 (6).

(1*S*,5*S*,6*R*,8*S*)-5-[(Methoxymethyl)oxy]-8-[9′-(9′-phenylxanthenyl)oxy]-2-oxabicyclo[3.2.1] octan-6-ol (6). To a solution of **5** (100 mg, 0.2 mmol) in THF/MeOH/H_2O, 5:4:1 (5 mL) was added 1M NaOH (1 mL), and the mixture was stirred for 45 min at rt. After being quenched with saturated $NaHCO_3$ (4 mL) and extracted with CH_2Cl_2 (3 × 5 mL), the combined organic phases were dried (Na_2SO_4) and evaporated, and the residue was purified by FC (hexane/EtOAc, 1:1, 1% Et_3N) to give **6** (92 mg, quantitative) as a white foam.

TLC (hexane/EtOAc, 1:1): Rf = 0.37. ^{1}H NMR (300 MHz, $CDCl_3$): δ 1.30−1.42 (*m*, 1H); 1.67 (*ddd*, *J* = 15.2, *J* = 4.0, *J* = 1.8, 1H); 2.07−2.15 (*m*, 1H); 2.52−2.63 (*m*, 1H); 3.01 (*d*, *J* = 2.6, 1H); 3.17 (*d*, *J* = 5.9, 1H); 3.40 (*m*, 1H); 3.52−3.60 (*m*, 4H); 3.84 (*dt*, *J* = 12.1, *J* = 4.0, 1H); 4.59, 4.67 (2*d*, *J* = 7.3, 2H); 4.72−4.76 (*m*, 1H); 6.99−7.47 (*m*, 13H). ^{13}C NMR (75 MHz, $CDCl_3$): δ 30.63 (*t*); 33.34 (*t*); 55.59 (*q*); 59.15 (*t*); 73.61 (*d*); 75.87 (*d*); 76.05 (*s*); 81.96 (*d*); 84.49 (*s*); 91.13 (*t*); 116.04, 116.56 (2*d*); 122.45 (*s*); 122.81, 123.14 (2*d*); 124.10 (*s*); 126.55, 126.99, 127.64, 129.27, 129.53, 130.52, 131.66 (7*d*); 149.10, 150.93, 151.47 (3*d*). IR ($CHCl_3$): 3484 *w*, 3002 *m*, 1604 *m*, 1574 *m*, 1479 *s*, 1448 *s*, 1319 *m*, 1296 *m*, 1236 *s*, 1138 *m*, 1119 *m*, 1101 *m*, 1064 *m*, 1026 *m*, 936 *w*, 900 *w*, 874 *w*. MS (EI): 459 (<1, $M^+ - 1$), 415 (<1), 398 (<1), 302 (<1), 257 (100), 181 (7), 45 (20).

(1*S*,5*S*,6*R*,8*S*)-6-{[(2′-Cyanoethoxy)(diisopropylamino)phosphino]-oxy}-5-[(methoxymethyl)oxy]-8-[9′-(9′-phenylxanthenyl)oxy]-2-oxabicyclo[3.2.1]octan (7). To a solution of **6** (550 mg, 1.19 mmol) and diisopropylethylamine (0.6 mL, 3.57 mmol) in dry THF (8 mL) was added dropwise $ClP[(OCH_2CH_2CN)(NiPr_2)]$ (0.4 mL, 1.78 mmol). The mixture was stirred for 1.5 h at rt, and then another portion of $ClP[(OCH_2CH_2CN)(NiPr_2)]$ (134 μL, 0.6 mmol) was added. After being stirred for a total of 6 h, the solution was diluted with CH_2Cl_2 (50 mL) and extracted with saturated $NaHCO_3$ (30 mL). The aqueous phase was washed twice with CH_2Cl_2 (30 mL), the combined organic phases were dried (Na_2SO_3) and evaporated, and the residue was purified by FC (hexane/EtOAc, 2:1, 1% Et_3N) to give **7** (718 mg, 91%) as a white foam.

TLC (hexane/EtOAc, 2:1): Rf = 0.48. ^{1}H NMR (300 MHz, $CDCl_3$): δ 1.16−1.31 (*m*, 13H); 1.56−1.72 (*m*, 1H); 1.90−1.98 (*m*, 1H); 2.30−2.45 (*dddd*, *J* = 21.1, *J* = 15.8, *J* = 10.5, *J* = 5.8, 1H); 2.55−2.61 (*m*, 2H); 2.87−2.93 (*m*, 1H); 3.17−3.19 (2*s*, 3H); 3.25 (*m*, 1H); 3.40−3.90 (*m*, 5H); 4.05, 4.07, 4.38, 4.40 (4*d*, *J* = 7.3, 2H); 4.61−4.74 (*m*, 1H); 6.87−7.40 (*m*, 13H). ^{13}C NMR (75 MHz, $CDCl_3$): δ 20.31 (*t*); 20.43 (*dt*, *J* = 7.3); 24.32, 24.42, 24.44, 24.52, 24.55, 24.60, 24.65 (7*q*); 32.94, 32.96 (2*t*); 33.96 (*dt*, *J* = 3.05); 34.28 (*t*); 43.23, 43.25 (2*dd*, *J* = 12.8); 54.99, 55.01 (2*dq*, *J* = 6.7); 57.76 (*dt*, *J* = 20.7); 58.50 (*dt*, *J* = 18.3); 59.64 (*t*); 75.91, 75.94 (2*s*); 76.36, 76.46 (2*d*); 77.04 (*dd*, *J* = 17.7); 77.47 (*dd*, *J* = 13.4); 78.80, 78.94 (2*d*); 85.15 (*ds*, *J* = 7.3); 85.26 (*ds*, *J* = 6.1); 92.41, 92.61 (2*t*); 116.18, 116.22, 116.52, 116.57 (4*d*); 117.51, 117.55 (2*s*); 122.38, 122.53 (2*s*); 123.17, 123.18, 123.21, 123.24 (4*d*); 124.10, 124.18 (2*s*); 126.62, 126.65, 127.29, 127.31, 127.59, 129.45, 129.51, 129.64, 130.69, 130.78, 131.49, 131.53 (12*d*); 148.47, 148.48, 151.12, 151.15, 151.62, 151.64 (6*s*). ^{31}P NMR (202 MHz, $CDCl_3$): 150.47, 150.58. IR ($CHCl_3$): 3070 *w*, 2968 *m*, 1603 *m*, 1574 *m*, 1478 *m*, 1447 *s*, 1365 *m*, 1319 *m*, 1297 *m*, 1236 *s*, 1182 *m*, 1148 *m*, 1118 *m*, 1101 *s*, 1074 *s*, 1043 *s*, 1026 *m*, 978 *m*, 937 *m*, 910 *w*, 896 *m*, 874 *w*, 830 *m*. MS (LSIMS): 661 (2, $M^+ + 1$), 600 (<1), 403 (1), 257 (100), 201 (11).

The synthesis of oligonucleotides was performed on the 1.3, 1, and 0.2 μmol scale on a Pharmacia LKB Gene Assembler Special and Applied Biosystems Expedite Nucleic Acid Synthesis System using standard phosphoramidite chemistry. The phosphoramidites of the natural nucleosides as well as the nucleosides bound to CPG solid support were from Glen Research. The solvents and reagents used for the synthesis were prepared according to the manufacturer's indications. After the synthesis, the oligonucleotides were detached and deprotected in concentrated aqueous ammonia (16 h at 55 °C) and filtered through Titan HPLC filters, Teflon, 0.45 μm, Infochroma AG. HPLC was performed on an Äkta Basic 10/100 system from Amersham Pharmacia Biotech.

Thermal denaturation experiments (T_m curves) were carried out on a Varian Cary 3E UV/vis spectrophotometer. Absorbances were monitored at 260 nm, and the heating rate was set to 0.5 °C/min. A heating−cooling−heating cycle in the temperature range 0−90 °C or 90−0 °C was applied. T_m data were determind from the first derivative of the absorbance melting curves using the Varian WinUV software. For temperatures <20 °C, nitrogen was passed through the spectrophotometer to avoid H_2O condensation on the cuvettes. To avoid evaporation of the solutions, a few drops of dimethylpolylsiloxane were added on top of the samples in the cell.

Acknowledgment. We thank the Swiss National Science Foundation (Grant No. 20-63582.00) for financial support.

Supporting Information Available: ^{1}H NMR spectra of compounds **4**−**7**, synthesis and MS analytical data of all oligonucleotides used, and the original UV melting curves to the derivatives depicted in Figures 2 and 3 (PDF). This material is available free of charge via the Internet at http://pubs.cs.org.

JA035313J